INTERNATIONAL JOURNAL OF INTEGRATED ENGINEERING
ISSN: 2229-838X e-ISSN: 2600-7916

IJIE

Vol. 17 No. 1 (2025) 117-129
https://publisher.uthm.edu.my/ojs/index.php/ijie

CFD Simulations of Natural Cross Ventilation in Building with Different Opening Positions and Louver Slat-Angles in Moderately-Dense Urban Area

Lip Kean Moey[1]*, Hussein Abubakar Kassam[2], Kah Yau Yap[2], Yew Hin Fam[2], Vin Cent Tai[1], Tze Fong Go[3], Mohammad Hossein Yazdi[4]

[1] *Centre for Sustainable Design, Modelling and Simulation, Faculty of Engineering, Built Environment & Information Technology, SEGi University, 47810, Selangor, MALAYSIA*
[2] *Faculty of Engineering, Built Environment & Information Technology, SEGi University, 47810, Selangor, MALAYSIA*
[3] *Centre of Advanced Materials and Sustainable Manufacturing, Faculty of Engineering, Built Environment & Information Technology, SEGi University, 47810, Selangor, MALAYSIA*
[4] *College of Engineering and Technology, University of Technology and Applied Sciences, PO Box 74, Al-Khuwair, Muscat 133, OMAN*

*Corresponding Author: moeylipkean@segi.edu.my
DOI: https://doi.org/10.30880/ijie.2025.17.01.010

Article Info

Received: 19 August 2024
Accepted: 18 February 2025
Available online: 30 April 2025

Keywords

Natural cross ventilation, louver slat-angle, urban area, dimensionless volume flow rate, CFD simulations

Abstract

In this study, CFD simulations with ANSYS 2021 R2 were performed on a targeted building with natural cross ventilation in urban area. The arrangement of the nine buildings has the planar area ratio of 0.25, which is considered moderately dense. The targeted building was with respective windward and leeward opening in the Middle-Middle, Top-Top, Bottom-Bottom, Bottom-Top, and Top-Bottom. The openings were without louver (NL) and equipped with louvers of 0°, 15°, 30°, or 45° slat-angles. The Grid Convergence Index (*GCI*) analysis found that the basic grid-size of 7.98 million cells is suitable for the simulation. Subsequent Factor of 2 (*FAC2*) analysis shows that the *Sk-ε modified coefficient* with enhanced wall function is the most suitable turbulence model. The simulations show maximum dimensionless streamwise mean velocities (U/U_{ref}) and dimensionless kinetic energies (k/U_{ref}^2) occurred at respective level of the windward opening; and that increasing the louver slat-angle caused maximum U/U_{ref} and k/U_{ref}^2 decreased at increasing Y/H. The Y/H against U/U_{ref} and k/U_{ref}^2 for Top-Top and Top-bottom opening configuration were of high values for each louver slat-angle. Windward with Top opening achieved higher dimensionless volume flow rate (*DFR*); with Top-Top opening configuration showed highest *DFR* for NL followed by louver slat-angle of 0^o to 45^o. Bottom-Bottom opening configuration shown significantly lowest *DFR*. This study demonstrates the importance of considering the effects of opening positions and louver slat-angles in an urban area on the performance of the natural cross ventilation for buildings.

1. Introduction

Natural resources depletion and global warming are posing serious concerns [1]. Over 40% of world energy consumption are contributed by building sector [2]. Energies utilised for ventilation, heating, and cooling contribute to over 60% of total building-energy consumption [3]. As 60% of estimated eight billion world population is anticipated to stay in cities by 2030, further worldwide urbanization with greater vehicle emissions and urban energy consumptions would occur [4]. Natural ventilation has, therefore, increasingly popular for reducing energy consumption such as with creation of new area known as "low energy architecture". High-density buildings with efficient designs are best for solving urban's need for shelter, work, and activity spaces. Residential buildings normally rely on natural ventilation to attain suitable indoor environments so as to conserve on energy utilization [5]. Failures in ventilation design can drastically affect lifetime performance and running cost of building. Moreover, the choice of the ventilation system(s) has to be decided during the early building-design phase as the setting-ups of the ventilation system(s) will influence the building-design itself [6]. Detailed understanding of in-building's airflow created by pressure differentials caused by wind and/or buoyancy-forces is required for achieving proper design of natural ventilation in buildings.

Increase in energy consumption is most directly related to current climate change. Rising temperatures during hot-season tend to increase cooling demand. The added timing and intensity uncertainties of future temperature changes driven by increasing global greenhouse gas emissions (due to use of fossil fuel) further aggravate the damages on future climates. The current urbanization trend has been impacting on the living quality; against the consistent calls to make cities and communities sustainable as contained in SDG 11 [7]. While being cheapest way to provide interior cooling of the buildings, naturally induced airflow can be extremely complex even for buildings with simple geometries. It is, therefore, important to understand outdoor wind-flow and indoor air-flow interactions through *CFD* simulations.

Kosutova et al. [8] conducted wind-tunnel experiments and *CFD* simulations of a cross ventilated building equipped with louvers. The four opening positions studied were: (i) openings at the centre, (ii) upper and (iii) lower part of the windward and leeward facades and (iv) one opening at the upper part of the windward facade and one opening at the lower part of the leeward facade. The 3D Reynolds-averaged Navier-Stokes (*RANS*) simulations were performed with Renormalization group (*RNG*) *k-ε*, *SST k-ω*, and Reynolds stress model (*RSM*) turbulence models and validated with wind-tunnel experiments. The experimental results showed that largest velocities occurred in upper openings of the facade. The *CFD* simulations showed *RSM* provided best agreement with the experimental data. The *CFD* simulations also showed that the highest *DFR* of 0.69 was obtained in building with louvered openings in the upper part of the facade.

Moey et al. [9] investigated effects of opening configuration on the indoor airflow of a naturally ventilated isolated building model with 3D RANS turbulence model, specifically the Shear Stress Transport (SST) k-ω. The different windward and leeward opening configurations studied were three cases of aligned openings and four cases of non-aligned openings. The simulation results indicated that the indoor air velocity and pressure distribution were highly dependent on both windward and leeward opening configurations; and different opening configuration influenced on the forming of in-building recirculation zone. Compared to openings located near the ground, near roof openings generated 6.52% higher ventilation rate. The study concluded that opening configurations affected internal airflow pattern, air recirculation, and ventilation rate for a naturally cross ventilated building.

Tai et al. [10] conducted *CFD* simulations on cross ventilation of an isolated building equipped with windward and leeward opening configurations at: (i) center-center, (ii) top-top, (iii) bottom-bottom, (iv) top-bottom and (v) bottom-top for both No-Louver (NL) and louvers with slat-angle of 0°, 15°, 30° and 45°. Atmospheric boundary layer (ABL) condition was applied at inlet of flow domain, and *RNG k-ε* turbulence model with Enhanced Wall Treatment (*EWT*) was employed. The simulations showed highest *DFR* of 0.719 was achieved by top-top configuration with NL.

Shirzadi et al [11] proposed a novel and systematic methodology for enhancing accuracy of the *k-e* model for applications in urban study such as cross ventilation in sheltered buildings. A microclimate *CFD* model for cross ventilation was firstly constructed for validating with experimental results of Tominaga and Blocken [12]. The *k-e* model's closure coefficients were modified with a stochastic optimization and Monte Carlo Sampling techniques. The probability density function (PDF) of all the closure coefficients were then provided to the optimizer for defining proper objective function in terms of different validation metrics. The modified coefficients from the developed systematic method were found simulating cross ventilation phenomena inside the building successfully with less than 8% airflow rate prediction error compared to the experimental results.

The slat-angle of the louver affects the pressure differential across the opening, thus, influences on the indoor air-velocities and airflow pattern. Furthermore, the opening position-configurations influence indoor air velocity and airflow pattern, as well as the airflow rates through the building. However, to the best of authors knowledge, study on the building arrangements in moderately-dense urban environment for evaluating parameters such as louver slat-angle and opening position on building ventilation is limited in the literature. Therefore, this study

Int. Journal of Integrated Engineering Vol. 17 No. 1 (2025) p. 117-129

aims to (i) analyse the dimensionless streamwise mean velocities (U/U_{ref}), and dimensionless TKE/U_{ref}^2 for a naturally cross ventilated building in moderately-dense urban area; and (ii) evaluate the dimensionless flow rate (*DFR)* for a targeted building with natural cross ventilation without and with louvers of different slat-angles for different opening positions. The targeted building height was set to 2H to demonstrate a warehouse/factory with an urban environment. This present study is further broken down into various sections. In section 2, information on numerical study such as simulation cases, computational domain, boundary conditions, and grid sensitivity analysis will be discussed. Additionally, section 3 will present and analyze the simulation results. Lastly, the overall research achievement will be concluded in section 4.

Nomenclature

C_μ	model constant
Q	volume flow-rate
r_w	wall-opening porosity
U/U_{ref}	Dimensionless streamwise mean velocities, normalized speed, mean streamline velocity ratio, or average velocity profile
k/U_{ref}^2	dimensionless *TKE*
U_{ABL}^*	ABL friction velocity or wind speed at reference height
U	inlet velocity profile or 3Dstreamwise velocity vector
U_{ref}	applied reference velocity
U_H	Wind speed at the building height (or streamwise-velocity)
Z_{ref}	reference height

Greek letters

ε	*TKE*/turbulent dissipation-rate
κ	Von Karman constant
λ_p	planar area index/ratio

Abbreviations

ABL	Atmospheric Boundary Layer
BOI	Body-of-influence
CFD	Computational fluid dynamics
DFR	Dimensionless volume flow-rate
EWT	Enhanced Wall Treatment
RANS	Reynolds-averaged Navier-Stokes
RNG	Renormalization group
RSM	Reynolds stress model
SST	Shear-stress transport

2. Methodology

2.1 Model Geometry

For model validation, various turbulence models were performed for a single-zone targeted building model of 200 mm × 200 mm × 160 mm (L × W × H), with wall thickness of 3 mm with reference to Shirzadi et al.'s study [11]. The targeted building for this analysis was without louver and with wall-opening porosity, r_{w2} = 10.35% ($= \frac{0.092 \text{x} 0.036}{0.16 \text{x} 0.2}$ x 100%). The targeted building was surrounded by eight similar cubic buildings without opening; spaced at a distance similar to building width of 1.25H which is 200 m as shown in Fig. 1. Thus, the planar area ratio, λ_p= 0.25 ($= \frac{0.20 \text{x} 0.20}{(0.20+0.20)(0.20+0.20)}$); indicating the targeted building was located within a moderately-dense area [11].

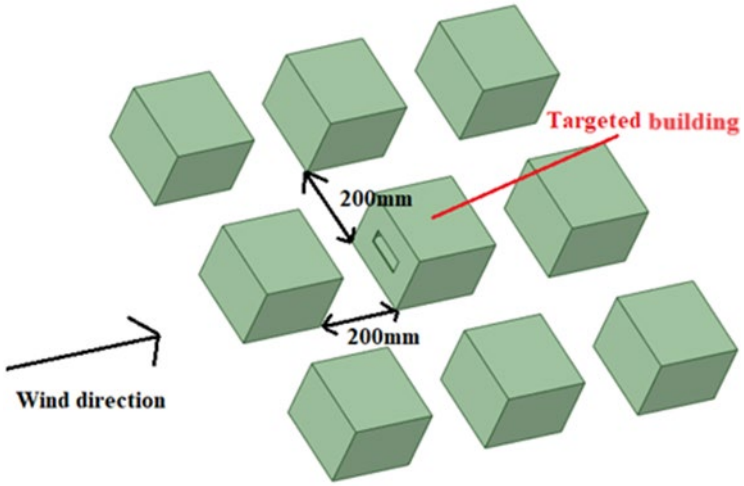

Fig. 1 *Arrangement of the targeted building*

2.2 Computational Flow Domain and Body-of-Influence (BOI)

With reference to Shirzadi et al.'s study, the computational flow domain as shown in Fig. 2 was with upstream length of 5H of 800 mm; where H = height of the targeted building of 160 mm for avoiding unintended stream-wise gradients in the approach-flow. The targeted building was also with distance of 5H of 800 mm to lateral sides and to top of flow domain, while the flow domain's downstream length was 15H of 2400 mm. This resulted in a computational flow domain with total flow domain dimensions of 2.6 m × 4.2 m × 0.96 m [11].

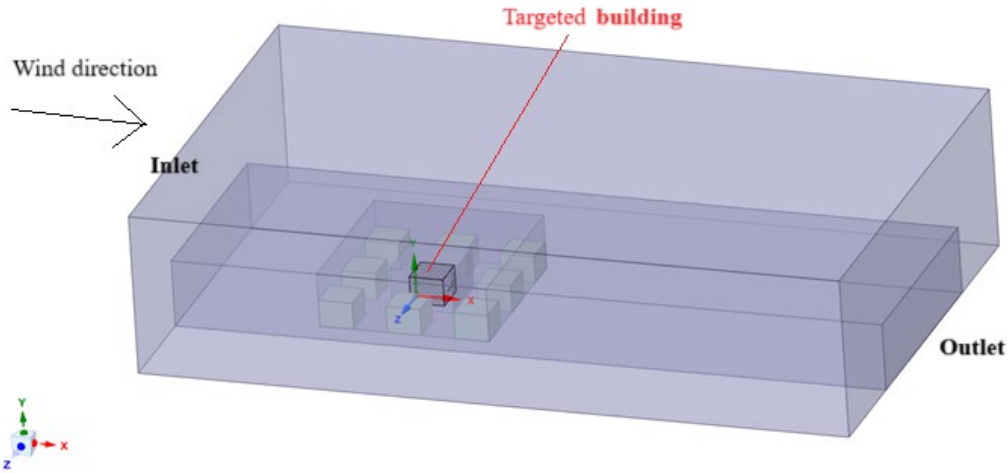

Fig. 2 *Dimensions of the computational domain*

Mosaic™ meshing technology that is able to construct high quality octree hexahedrons for the bulk region was applied to the model-geometry. It also allows automatic connection of all element types to produce high quality meshes, and to efficiently solve fluid-flow around highly complex geometries. A tetrahedral mesh was firstly applied to the model-geometry with the scope-sizing function to be subsequently converted into poly-hexcore [10]. Eight prism layers with first cell height of 0.0002 m were applied to targeted building, surrounding buildings, and ground to yield the desired mesh quality and to ensure Wall Y+ not exceeding 5. The skewness for all numerical cases were controlled to be below 0.75.

2.3 Atmospheric Boundary Layer (ABL) Condition

The fluid used in this study was air with 1.225kg/m^3 density and 1.789x10^{-5} kg/ms dynamic viscosity. An ABL file was applied at user-defined functions (*UDF*) to create velocity profile at inlet of flow domain. The key boundary conditions include [8]:

i) ABL friction velocity (or wind speed at reference height),

Int. Journal of Integrated Engineering Vol. 17 No. 1 (2025) p. 117-129

$$U^*_{ABL} = \frac{\mathrm{U_{ref}} \times \kappa}{\log(\frac{\mathrm{Z_{ref}} + \mathrm{Z_0}}{\mathrm{Z_0}})} \quad (1)$$

where U_{ref} = 4.3m/s, Z_{ref} = building or reference height = 0.15 m, κ = 0.4, and Z_0 = height of aerodynamic roughness = 0.0024 m.

ii) wind profile at lower part of ABL was represented by a power law profile:

$$\frac{U(z)}{U_H} = (\frac{z}{H})^{0.25} \quad (2)$$

where $U_{(z)}$ = streamwise velocity at z, and U_{ref} = velocity at building height H = 4.3m/s

iii) measured TKE's vertical profile was approximated by exponential formulation:

$$\left(\frac{k\,(z)}{{U_H}^2}\right) = 0.033e^{-0.32\left(\frac{z}{H}\right)} \quad (3)$$

iv) TKE dissipation-rate can be approximated by:

$$\varepsilon(z) = C_\mu^{\frac{1}{2}} k(z) \frac{U_H}{H} \alpha(\frac{z}{H})^{z-1} \quad (4)$$

where C_μ= model constant = 0.09; and α = 0.25.

The flow domain's top and side walls were set with zero normal gradients and velocities to represent the zero-shear. While the outlet was set to be pressure-outlet, the inlet was set to be velocity-inlet having velocity magnitude, *TKE* and *ε* were provided by the ABL file, while *TKE* was with reference to Shirzadi et al.'s 2018 study [11].

The turbulent kinetic energy, k was found by measuring the fluctuation in velocity by using equation (3). Then, the turbulent dissipation rate, ε was obtained by using equation (4) while the specific dissipation rate ω was obtained by using equation (5) whereby Cμ was 0.09 [13].

2.4 Solver Setting

ANSYS 2021 R2 was used for all CFD simulation cases. 3 k-epsilon (2 eqn), *Skε modified coefficient* turbulence model were employed with *EWT*; as *EWT* yielded good wall Y+ of below 5. The values of standard *Skε* coefficient that showed better agreement with the experimental data were C_μ = 0.09, $C_{\varepsilon1}$ = 1.44, $C_{\varepsilon2}$ = 1.92, σ_k = 1, σ_ε = 1.3; while the values of *modified Skε coefficient* obtained were even better with C_μ = 0.05, $C_{\varepsilon1}$ = 1, $C_{\varepsilon2}$ = 3.2, σ_k = 0.8, σ_ε = 0.358584. It was found that the values of *modified Skε coefficient* has better performance as it has better FAC2 and RMSE compared to standard *Skε* coefficient [13]. "SIMPLE" scheme was selected for "Pressure-Velocity Coupling", "Least Squares Cell Based" was selected as "Gradient" under Spatial Discretization, and "Second Order Upwind" were selected for "Pressure", "Momentum", "Turbulent Kinetic Energy", and "Turbulent Dissipation rate". Standard Initialization was used with convergence criteria of 1 x 10^{-4} for continuity, x, y, z-velocity, k, and epsilon. All the solutions converged after approximately 800 iterations.

2.5 Sensitivity Analysis

Grid sensitivity analysis (in terms of U/U_{ref} along lines at the centre-plane) was conducted on coarse, basic, and fine grids in which the basic grid is refined or coarsened with linear grid refinement factor (r) of about $\sqrt{2}$. Reference-grid for all the cases was determined by using *GCI* that estimates the error of the U/U_{ref}. *GCI* can be calculated with formula as shown, where factor of safety, F_s = 1.25 for 3 or more grids, r = $\sqrt{2}$, and formal order of accuracy, p = 2 when the "Second-order discretization scheme" is used [10].

$$GCI = SF\,|\frac{r^p\frac{U_{course}-U_{fine}}{U_{ref}}}{r^p-1}| \quad (5)$$

Grid sensitivity analysis was conducted using coarse grid (with 5.38 million cells), basic grid (with 7.78 million cells), and fine grid (with 12.83 million cells) on the targeted building at X/D = 0.2, 0.4, 0.6, and 0.8 respectively. The corresponding graphs of grid sensitivity analysis for *Skε modified coefficient* are shown in Fig 3. The average *GCI* for the *Reliazable, Skε*, and *Skε modified coefficient* turbulence models were 2.8661, 1.2044, and 1.4190 respectively for coarse vs fine, and 0.6032, 0.8610, and 0.6129 respectively for basic vs fine. The average *GCIs* for basic vs. fine grids were all lower than the average *GCIs* for coarse vs. fine grids. The average *GCIs* for basic vs. fine grids were all less than 1 which indicating the basic grid can be used for all subsequent simulations in this study.

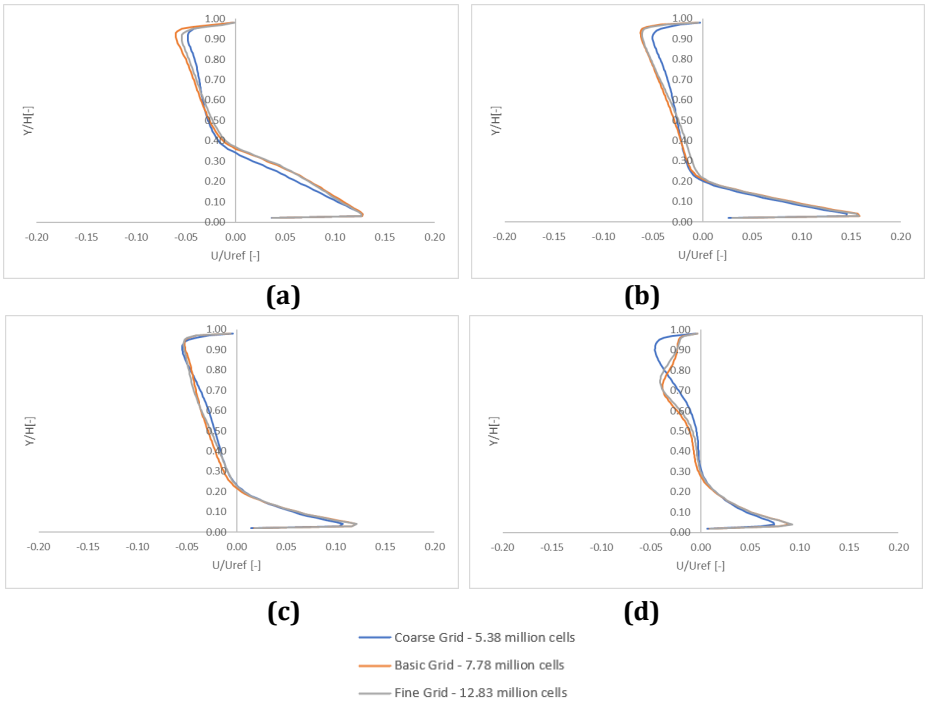

Fig. 3 *Grid sensitivity analysis for Skε modified coefficient at (a) X/D = 0.2; (b) X/D = 0.4; (c) X/D = 0.6; (d) X/D = 0.8*

2.6 Modal Validation

Two quantitative metrics used for model validation were Factor of two of observation (*FAC2*) and Root Mean Square Error (RMSE). *FAC2* is for validating effectiveness of the turbulence models, and was accepted by researchers [10, 13]. *FAC2* can be calculated with:

$$FAC\ 2 = \frac{1}{n}\sum_{i=1}^{n} N_i$$
$$where, N_i = \begin{cases} 1 & if\ 0.5 \le \frac{P_i}{O_i} \le 2 \\ 0; & else \end{cases} \quad (6)$$

whereby P_i is the predicted value generated from this study while O_i is the experimental result from wind tunnel experiment [11]. Observed *FAC2* value is acceptable when it is between 0.5 and 2. An ideal data set have *FAC2* of 1.

Data for the *FAC2* analysis of *Reliazable, Skε*, and *Skε modified coefficient* were obtained with Equation 6. The *FAC2* of the turbulence models in this study was versus Shirzadi et al. 2018's [11] experimental data at X/D = 0.125, 0.5, and 0.875. For *Realizable* and *Skε* turbulence models, *FAC2* of the study's data versus Shirzadi et al. 2018's [11] experimental data (*Study vs Exp*) respectively shows low average of 0.4 and 0.24, respectively. *Skε*

Int. Journal of Integrated Engineering Vol. 17 No. 1 (2025) p. 117-129

modified coefficient, on the other hand, shows better results with *FAC2* of 0.45 and has the similar trend as Shirzadi et al. 2018's *Skε modified coefficient*. Therefore, *Skε modified coefficient* with basic grid will be used for all subsequent simulations in this study.

2.7 Geometry and Arrangement of the Simulation Model

CFD simulations were conducted for a single-zone targeted building of 0.20 m × 0.20 m × 0.32 m, the height of 2H was to demonstrate a warehouse with an urban environment. The openings were equipped with NL and louvers of 0.75 mm thickness with 0°, 15°, 30°, and 45° slat-angle [Fig. 4(a)] installed at windward and leeward opening positions of Middle-Middle, Top-Top, Bottom-Bottom, Top-Bottom, and Bottom-Top as shown in Fig. 4(b). The dimension of the opening positions of louvers at three different locations were shown in Fig. 4(c). The targeted building was surrounded by eight similar cubic buildings without opening with λ_p of 0.25.

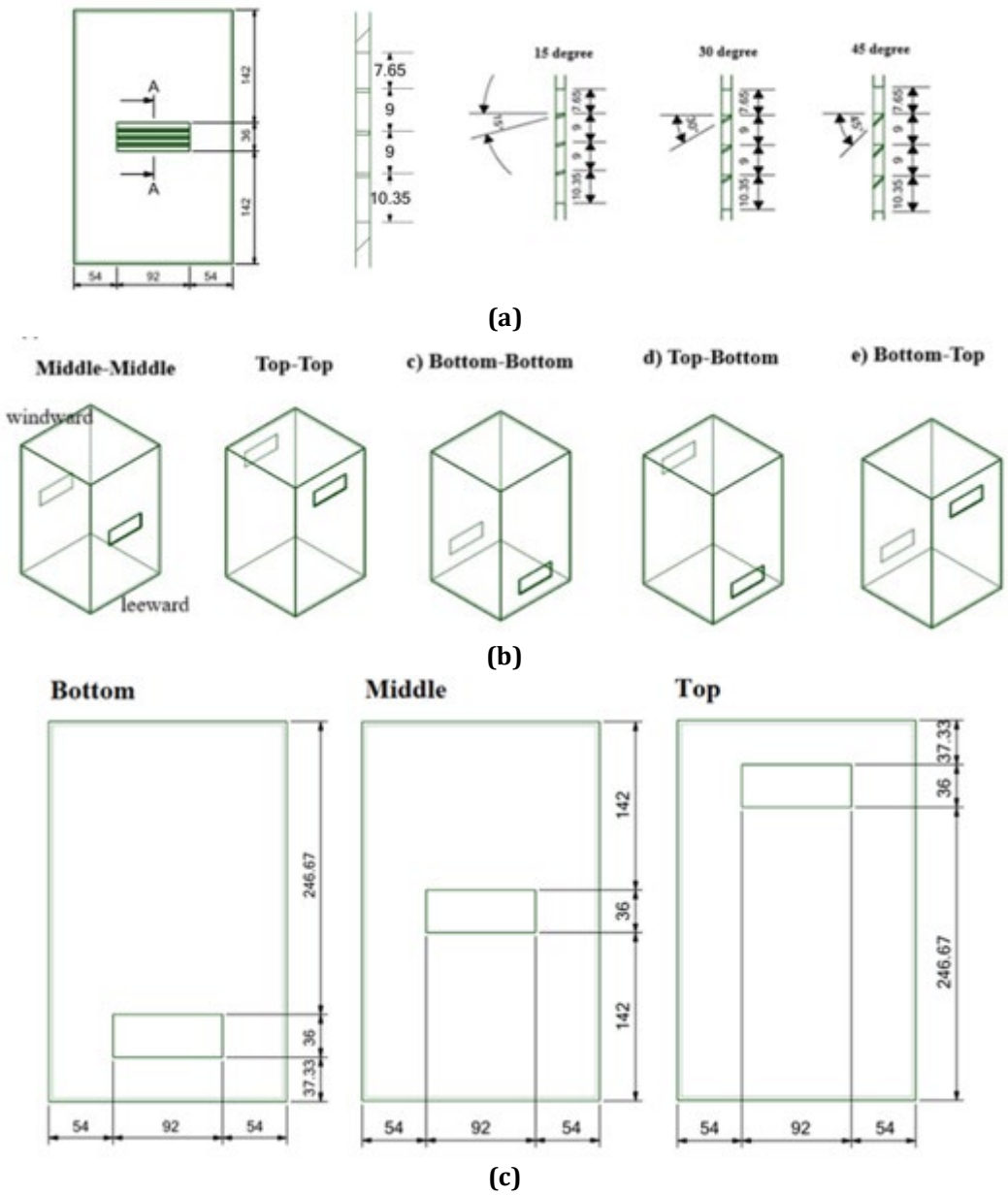

Fig. 4 *Details of targeted building with 2H (a) Details of louvers; (b) Opening positions; and (c) Dimension of openings position (all dimensions are in mm)*

Simulations were performed on 25 cases, as shown in Table 1. Contours of U/U_{ref}, TKE/U_{ref}^2 ; as well as bar-chart of *DFR* will be presented in the following section.

Table 1 *Simulation cases*

Case No.	Configuration of Opening Positions	Slat-Angle of Louvers
1	Middle-Middle	a) No-Louver (NL)
2		b) 0°
3		c) 15°
4		d) 30°
5		e) 45°
6	Top-Top	a) No-Louver (NL)
7		b) 0°
8		c) 15°
9		d) 30°
10		e) 45°
11	Bottom-Bottom	a) No-Louver (NL)
12		b) 0°
13		c) 15°
14		d) 30°
15		e) 45°
16	Top-Bottom	a) No-Louver (NL)
17		b) 0°
18		c) 15°
19		d) 30°
20		e) 45°
21	Bottom-Top	a) No-Louver (NL)
22		b) 0°
23		c) 15°
24		d) 30°
25		e) 45°

3. Simulation Results

3.1 Dimensionless Streamwise Mean Velocity (U/U_{ref})

Fig. 5. shows the patterns of Y/H against U/U_{ref} for all the 25 cases at X/D = 0.5 (i.e. at the middle of the targeted building). The configuration of the opening positions in Fig. 5(a) to 5(e) correlates with the behaviour of the U/U_{ref} distribution by determining where the maximum velocities occur within the building. Maximum U/U_{ref} occurred at respective level according to the windward opening (i.e. (a) at Middle level, (b) at Top level, (c) at Bottom level, (d) at Top level, (e) at Bottom level). Increasing the louver slat-angle from NL to 45° cause recorded maximum U/U_{ref} to decrease at increasing Y/H for each opening configuration. The decrease in recorded maximum U/U_{ref} was due to the increasing louver slat-angle from NL to 45° that acted to increase blockage to the effective opening area. The increased Y/H for the recorded maximum U/U_{ref} was due to the increasing louver slat-angle from NL to 45° that deflected the air upwards. The peak value of U/U_{ref} for the NL case is significantly higher compared to other configurations because the absence of louvers allows for unobstructed airflow, resulting in maximum velocity at the windward opening. In contrast, the introduction of louvers (even at lower angles) increases blockage, which reduces the effective opening area and subsequently lowers the maximum U/U_{ref}. The patterns of Y/H against U/U_{ref} for Top-Top and Top-bottom opening configuration were of similarly high values for each louver slat-angle.

Int. Journal of Integrated Engineering Vol. 17 No. 1 (2025) p. 117-129

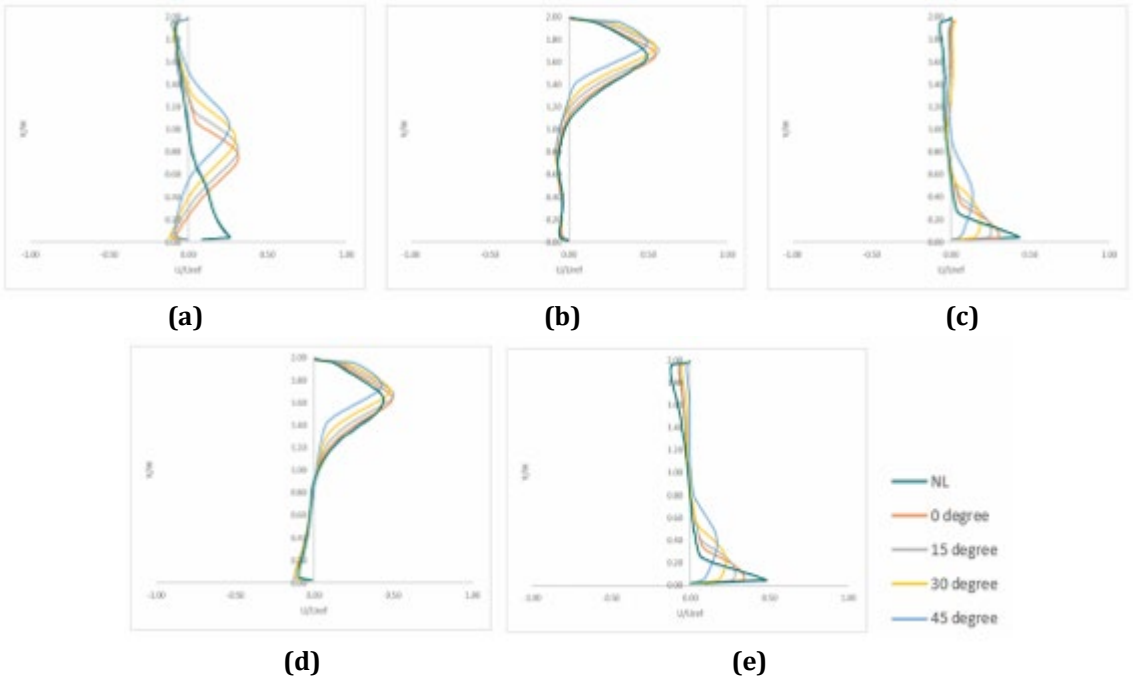

Fig. 5 *Y/H against U/U$_{ref}$ for NL and louver slat-angles of 0^o, 15^o, 30^o, and 45^o at X/D = 0.5 for (a) Middle-middle; (b) Top-top; (c) Bottom-bottom; (d) Top-bottom; (e) Bottom-top opening positions*

The dimensionless streamwise mean velocities is the measured mean streamwise velocity (U) divided by applied velocity at building height (U_{ref}) of 4.3m/s. Similar to Kosutova et al. [8] and Tai et al. [10] studies, the entering-jet is deflected upwards caused by tilting-up angle of the inlet louver and tilting-down angle of the outlet louver. From Table 2, external vortexes were formed at the back of the front building due to the winds flowing from top of the front buildings were blocked by the taller targeted building to flow downward prior to being directed to enter the targeted building through the windward opening as incoming flow. For Middle-Middle opening configuration, no internal recirculation zone was formed in the targeted building with NL. The presence of louvers diverted the entering flows upwards to form two recirculation zones inside the targeted building; with increasing louver slat-angles from 0^o to 45^o increase intensity of the recirculation zones formed. For Top-Top opening configuration, strongest single recirculation zone was formed in the targeted building with NL. Presence of louvers directed more flows to the ceiling due to the Coanda effect as observed in Tominaga and Blocken's 2016 study [14]. As the louvers slat-angle increased from 0^o to 45 ^{o}, the Coanda effects were stronger in minimising intensities of the single recirculation zones formed in the region below the Top-Top opening. Slower outflow from the targeted building were also observed with increasing louver slat-angle.

For Bottom-Bottom opening configuration, no internal recirculation zone was formed in the targeted building with NL. The presence of louvers diverted the entering flows upward to form one recirculation zone inside the targeted building with increasing louver slat-angle from 0^o to 45^o increase intensity of the recirculation zone formed in the region above the Bottom-Bottom opening. Weaker external vortexes show lower speeds of the outflow from the targeted building. At Top-Bottom opening configuration, strongest single recirculation zone was formed in the targeted building with NL. Similar with Top-Top opening configuration, presence of louvers minimise the intensity of the single recirculation zone formed below the windward opening and allowed slower outflow from the targeted building as the louver slat-angle increased from 0^o to 45 ^{o}. For Bottom-Top opening configuration, strongest single recirculation zone was formed in the targeted building with NL. Presence of louvers minimise the intensity of the recirculation formed in the targeted building and allowed slower outflow from the targeted building as the louvers slat angle increased from 0^o to 45 ^{o}.

Table 2 *U/U_{ref} contours (with streamlines) for NL and louver slat-angles of 0°, 15°, 30°, and 45° for (a) Middle-middle; (b) Top-top; (c) Bottom-bottom; (d) Top-bottom; (e) Bottom-top opening positions*

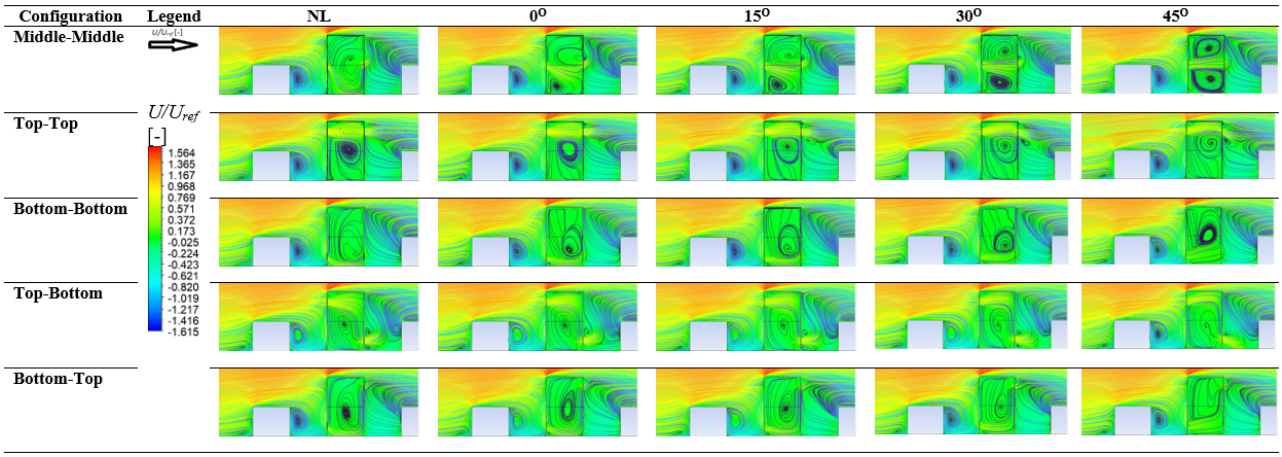

3.2 Dimensionless Turbulence Kinetic Energy (TKE)

Fig. 6 shows the patterns of Y/H against k/U_{ref}^2 for all the 25 cases at X/D= 0.5 (i.e. at the middle of the targeted building). From Fig. 6., maximum k/U_{ref}^2 occurred at respective level according to the windward opening (i.e. **(**a) at Middle level, (b) at Top level, (c) at Bottom level, (d) at Top level, (e) at Bottom level); as similarly indicated by the U/U_{ref} in Fig. 5. The minimal variation in airflow characteristics between the non-louvered (NL) and other louver configurations suggests that the louver angle has a limited effect on the turbulent energy in the flow field. Increasing the louver slat-angle from NL to 45° cause recorded maximum k/U_{ref}^2 to decrease at increasing Y/H for each opening configuration. The decrease in recorded maximum k/U_{ref}^2 was due to the increasing louver slat-angle from NL to 45° that acted to increase blockage to the effective opening area. The increased Y/H for the recorded maximum k/U_{ref}^2 was due to the increasing louver slat-angle from NL to 45° that deflected the air upwards. The patterns of Y/H against k/U_{ref}^2 for Top-Top and Top-bottom opening configuration were of similarly high values for each louver slat-angle; as similarly indicated by the U/U_{ref} in Fig. 5.

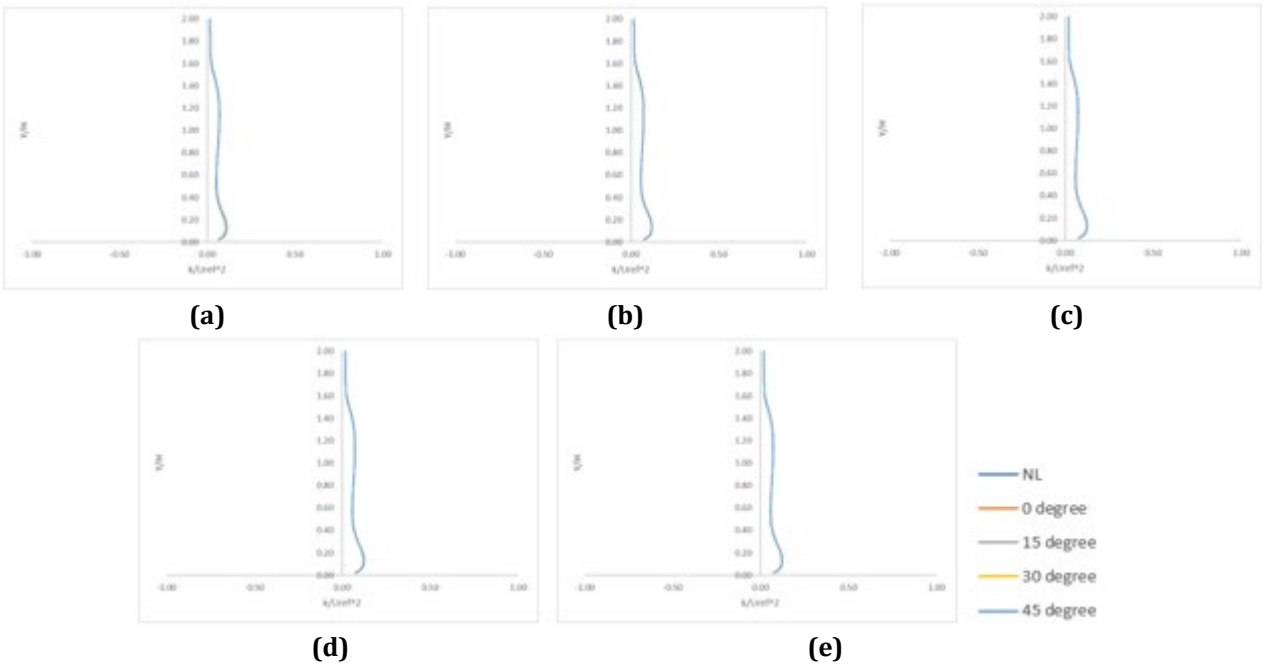

Fig. 6 *Y/H against k/U_{ref}^2 for NL and louver slat-angles of 0°, 15°, 30°, and 45° at X/D= -0.5 for (a) Middle-middle; (b) Top-top; (c) Bottom-bottom; (d) Top-bottom; (e) Bottom-top opening positions*

From Table 3, high k/U_{ref}^2 were observed at the windward top edge of the targeted building for all NL and louver cases due to flow separations as similarly observed by Tai et al. [10], Shirzadi et al. [15], and Kosutova et al. [8]. As the louver slat-angle increased from 0° to 45°, the k/U_{ref}^2 region in the targeted building after the

Int. Journal of Integrated Engineering Vol. 17 No. 1 (2025) p. 117-129

windward opening decreased with increasing louver slat-angle that acted as increasing blockages to the inflow air.

The larger internal k/U_{ref}^2 region were observed at Top-Top and Top-Bottom opening configuration due to no front surrounding building blocked the incoming flow to the windward opening. As expected, the Top-Top opening configuration showed highest k/U_{ref}^2 as there was also no blockage on the exiting flow by the building at the back of the targeted building. The k/U_{ref}^2 region size followed the trend of Fig. 7. Also, the larger k/U_{ref}^2 region size and magnitude correlated to the higher U/U_{ref} as shown in Fig. 5.

Table 3 *Dimensionless TKE contours for NL and louver slat-angles of 0°, 15°, 30°, and 45° for (a) Middle-middle; (b) Top-top; (c) Bottom-bottom; (d) Top-bottom; (e) Bottom-top opening positions*

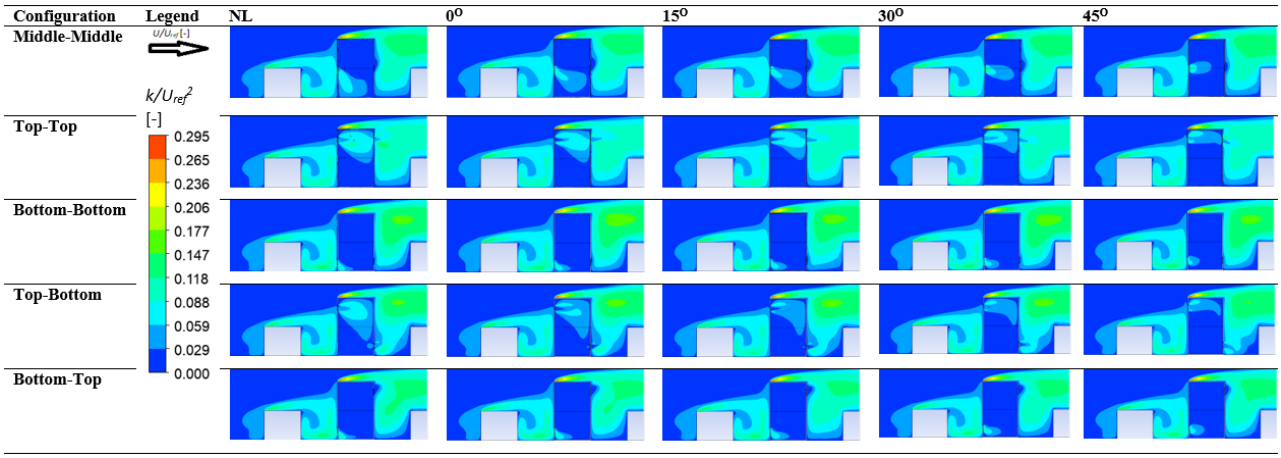

3.3 Dimensionless Volume Flow Rate (*DFR*)

DFR is calculated by using volume flow rate (Q) through the building divided by applied reference velocity of is 4.3 m/s and the area of opening of 0.003312 m² (A_w)

$$DFR = \frac{Q}{U_{ref} A_{inlet}} \tag{7}$$

From Fig. 7., windward with Top opening was found to achieve higher *DFR*. Top-Top opening configuration showed highest *DFR* for NL followed by louver slat-angle of 0° to 45°; respectively with value of 0.611, 0.591, 0.585, 0.553, and 0.487. Bottom-Bottom opening configuration shown significantly lowest *DFR* due to the air had to flow downwards from top of the front building to enter the targeted building at Bottom. The air would then exit from the targeted building slower through the Bottom as the air was blocked by the building behind.

Overall, the presence of louvers reduced the *DFR* as the louvers acted as blockage that reduced the effective opening area. *DFR* also decreased as the increasing louver slat-angle from 0° to 45° reduced the effective opening area further; as similarly observed by Tai et al. [10]. The trends of the *DFR* in this study generally are similar with results obtained by Tai et al. [10]; except the *DFR* difference between the different opening positions show bigger gaps due to the taller height of the targeted building.

It is interesting to observe that the *DFR* difference between targeted building with top windward opening and the targeted building with middle and bottom windward openings show bigger gaps; as compare to the results of Tai et al. [10] that showed smaller differences. It is observed that changed in louver slat angle from NL to 45° in opening positions of "Middle-Middle, "Bottom-Bottom", and "Bottom-Top" affected *DFR* by around 0.05 compared 0.1 for "Top-Top" and "Top-Bottom". This phenomenon could be due to effect of surrounding building that act as blockage to the air flow for the opening positions of "Middle-Middle, "Bottom-Bottom", and "Bottom-Top"; while the effect of louver slat-angle found by Tai et al. [10] showed larger reduction of around 0.4 from NL to 45° for isolated building. Overall, opening with NL generally showed higher *DFR* as observed by Kosutova et al. [8].

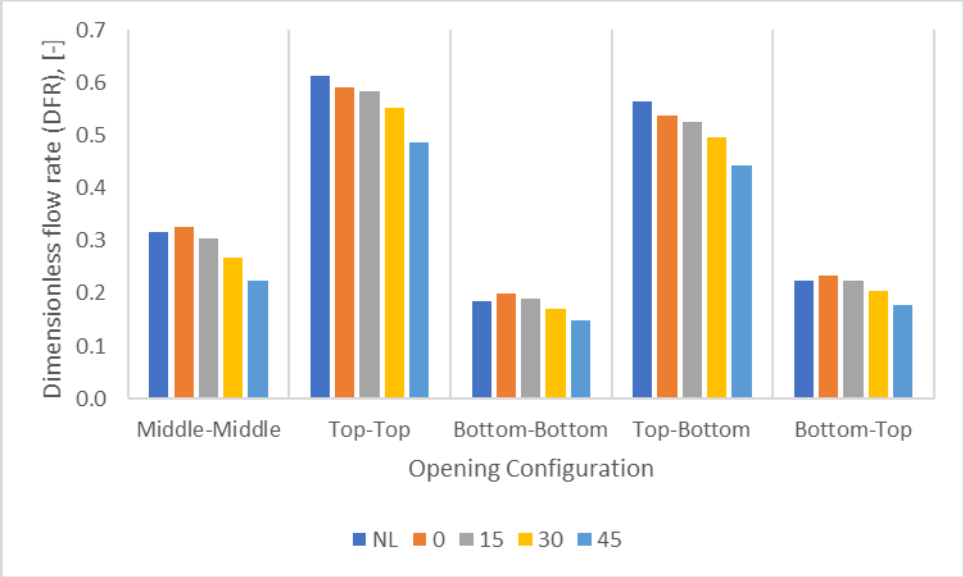

Fig. 7 *DFR for NL and louver slat-angles of 0°, 15°, 30°, and 45° for (a) Middle-middle; (b) Top-top; (c) Bottom-bottom; (d) Top-bottom; (e) Bottom-top opening positions*

4. Conclusion

CFD simulations were performed on a targeted building with natural cross ventilation in urban area. The arrangement of the nine buildings has the planar area ratio of 0.25, which is considered moderately dense. The Factor of 2 (FAC2) analysis found that Sk-ε modified coefficient with enhanced wall function as the most suitable turbulence model. The results show that maximum U/U_{ref} occurred at respective level of the windward opening (i.e. (a) at Middle level, (b) at Top level, (c) at Bottom level, (d) at Top level, (e) at Bottom level), maximum k/U_{ref}^2 was also similar to the U/U_{ref}. Furthermore, Windward with Top opening was found to achieve higher *DFR*. Bottom-Bottom opening configuration shown significantly lowest *DFR* due to the air has to flow downwards from top of the front building to enter the targeted building at the bottom. The reducing effective opening area created higher pressure difference that caused internal flows of higher k/U_{ref}^2 and U/U_{ref} with lower *DFR*. For future research works, it is recommended to consider the wind directions to further understand the impact of louvers on natural ventilation, thereby improving the performance of building ventilation in urban setting.

Acknowledgement

The project is funded by SEGi University, under the SEGi Internal Research Fund. Grant No: SEGiIRF/2023-Q1/FoEBEIT/031.

Conflict of Interest

The authors declare that there is no conflict of interest regarding the publication of the paper.

Author Contribution

The authors are responsible for the study conception, research design, data collection, data analysis, result interpretation and manuscript drafting.

References

[1] Marin-Silviu Nan, Emilia Dunca, Dana Stegaru & Anisor Parvu (2011). Solutions on site monitoring of environmental factors in Brownfields Ghelari. *International Journal of Energy and Environment, 5(1)*, 9–18.

[2] Shaban R. S. Aldhshan, Khairul Nizam Abdul Maulud, Wan Shafrina Wan Mohd Jaafar, Othman A. Karim & Biswajeet Pradhan (2021). Energy consumption and spatial assessment of renewable energy penetration and building energy efficiency in Malaysia: A review. *Sustainability, 13(16)*, 9244. https://doi.org/10.3390/su13169244.

[3] Nilofar Asim, Marzieh Badiei, Masita Mohammad, Halim Razali, Armin Rajabi, Lim Chin Haw & Mariyam Jameelah Ghazali (2022). Sustainability of heating, ventilation and air-conditioning (HVAC) systems in buildings - An overview. *International Journal of Environmental Research and Public Health, 19(2)*, 1016. https://doi.org/10.3390/ijerph19021016.

[4] Lan Chen, Jian Hang, Mats Sandberg, Leif Claesson & Silvana Di Sabatino (2017). The influence of building packing densities on flow adjustment and city breathability in urban-like geometries. *Procedia Engineering, 198*, 758–769. https://doi.org/10.1016/j.proeng.2017.07.127
[5] Mohd Farid Mohamed, Steve King, Masud Behnia & Deo Prasad (2011). A study of single-sided ventilation and provision of balconies in the context of high-rise residential buildings. *Low-Energy Architecture, 57*, 1954–1961.
[6] VES Ltd., (2022). Natural, mechanical and hybrid ventilation compared. https://ves.co.uk/hvac-solutions/school-ventilation/insights/natural-mechanical-hybrid-ventilation-compared/
[7] United Nation - Department of Economic and Social Affairs. (2023). Make cities and human settlements inclusive, safe, resilient and sustainable. https://sdgs.un.org/goals/goal11.
[8] Katarina Kosutova, Twan Van Hooff, Christina Vanderwel, Bert Blocken & Jan Hensen (2019). Cross-ventilation in a generic isolated building equipped with louvers: Wind-tunnel experiments and CFD simulations. *Building and Environment, 154*, 263–280. https://doi.org/10.1016/j.buildenv.2019.03.019.
[9] Moey Lip Kean, Chan Kar Lit, Tai Vin Cent, Go Tze Fong & Chong Perk Lin (2021). Investigation on the effect of opening position across an isolated building for wind-driven cross ventilation. *Journal of Mechanical Engineering and Sciences, 15(2)*, 8141–8152. doi: 10.15282/jmes.15.2.2021.14.0639.
[10] Tai Vin Cent, Wu Kai-Seun, Joseph, Mathew, Prasath Reuben, Moey Lip Kean, Cheng, Xinwei & Baglee David (2022). Investigation of varying louver angles and positions on cross ventilation in a generic isolated building using CFD simulation. *Journal of Wind Engineering and Industrial Aerodynamics, 229*, 105172. https://doi.org/10.1016/j.jweia.2022.105172.
[11] Mohammadreza Shirzadi, Parham Mirzaei, Mohammad Naghashzadegan & Yoshihide Tominaga (2018). Modelling enhancement of cross-ventilation in sheltered buildings using stochastic optimization. *International Journal of Heat and Mass Transfer, 118*, 758–772. https://doi.org/10.1016/j.ijheatmasstransfer.2017.10.107.
[12] Yoshihide Tominaga & Bert Blocken (2015). Wind tunnel experiments on cross-ventilation flow of a generic building with contaminant dispersion in unsheltered and sheltered conditions. *Building and Environment, 92*, 452–461. https://doi.org/10.1016/j.buildenv.2015.05.026.
[13] Li Qian, Tai Vin Cent, Moey Lip Kean, Go Tze Fong, Javad Safehian & Mohammad Hossein Yazdi (2023). Impact of planar area ratio and opening positions on natural cross ventilation performance in sheltered high-rise buildings: A simulation study. *Building and Environment, 245*, 110889. https://doi.org/10.1016/j.buildenv.2023.110889.
[14] Yoshihide Tominaga & Bert Blocken (2016). Wind tunnel analysis of flow and dispersion in cross-ventilated isolated buildings: Impact of opening positions. *Journal of Wind Engineering and Industrial Aerodynamics, 155*, 74–88. https://doi.org/10.1016/j.jweia.2016.05.007.
[15] Mohammadreza Shirzadi, Parham Mirzaei & Yoshihide Tominaga (2021). LES analysis of turbulent fluctuation in cross-ventilation flow in highly-dense urban areas. *Journal of Wind Engineering and Industrial Aerodynamics, 209*, 104494. https://doi.org/10.1016/j.jweia.2020.104494.